eCapillary: a disposable microfluidic extensional viscometer for weakly elastic polymeric fluids

Naureen S. Suteria, Siddhartha Gupta, Rajesh Potineni, Stefan K. Baier & Siva A. Vanapalli

Rheologica Acta

ISSN 0035-4511

Rheol Acta
DOI 10.1007/s00397-019-01149-9

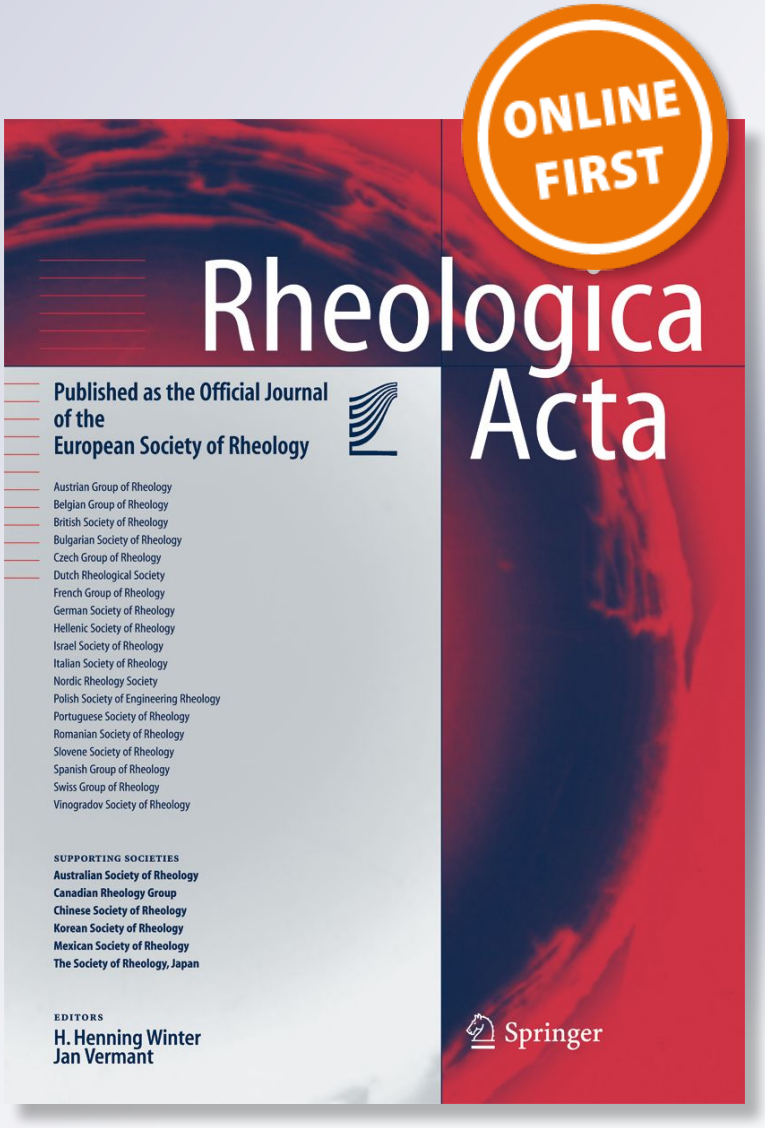

Springer

Rheologica Acta
https://doi.org/10.1007/s00397-019-01149-9

ORIGINAL CONTRIBUTION

eCapillary: a disposable microfluidic extensional viscometer for weakly elastic polymeric fluids

Naureen S. Suteria[1] · Siddhartha Gupta[1] · Rajesh Potineni[2] · Stefan K. Baier[2,3] · Siva A. Vanapalli[1]

Received: 27 September 2018 / Revised: 9 March 2019 / Accepted: 17 April 2019

Abstract

We report a disposable microfluidic extensional viscometer based on an optimized hyperbolic contraction–expansion geometry. This "eCapillary" device works by measuring pressure drop as a function of flow rate while accounting for viscous contribution to the pressure drop. The viscometer operates by applying a constant pressure and using an image-based approach to measure the flow rate. The device is fabricated entirely out of polydimethylsiloxane with no embedded sensors, making it disposable. We tested our approach using weakly elastic polymer solutions whose relaxation times were characterized by dripping-on-substrate rheology. Flow visualization was used to determine the onset of inertioelastic instabilities in the eCapillary device, thereby establishing the operating limits for extensional rheological measurements. Holography-based velocimetry analysis showed that extensional strain rate is uniform in a narrow section of the contraction throat necessitating correction for the shear contribution to the measured pressure drop. We observed the onset of extensional thickening to occur at Deborah number ≈ 1 and found that the apparent extensional viscosities are 2–4 orders of magnitude higher than the shear viscosities. Finally, we compared our data with those from other microfluidic extensional viscometers reported in the literature and found good agreement.

Keywords Semi-dilute polymer solution · Contraction flow · Microfluidic rheometry · Extensional viscosity · Flow visualization

Introduction

The resistance to extensional deformation by a viscoelastic fluid is characterized by its extensional viscosity (η_E) which depends on both the elongational strain rate ($\dot{\varepsilon}$) and the Hencky strain (ϵ_H). For the case of a cylindrical viscoelastic filament subjected to uniaxial extensional flow, its extensional viscosity is given by $\eta_E(\dot{\varepsilon}) = -(\tau_{zz}-\tau_{rr})/\dot{\varepsilon}$ where τ_{zz} and τ_{rr} are the axial and radial stresses in the fluid (Morrison 2001), respectively. The ratio of extensional viscosity to shear viscosity (η) is characterized by the Trouton ratio ($Tr = \eta_E/\eta$) (Trouton 1906). For a Newtonian fluid, $Tr = 3$; however, fluids with long-chain polymers (e.g., high molecular weight polyethylene oxide solutions), even at nominally dilute concentrations, have $Tr \approx 10^0$–10^4 (Anna and McKinley 2001; Tirtaatmadja and Sridhar 1993). This dramatic enhancement in η_E is due to extensional flow-induced stretching of long-chain polymers.

Characterization of the extensional viscosity of viscoelastic fluids is important for a wide range of applications. In polymer-melt applications such as fiber spinning, blow molding, and film extrusion, the extensional viscosity affects the kinematics of extrusion (Cogswell 1972) and dictates the final product quality (Gupta and Sridhar 1998). Likewise in printing applications, the extensional viscosity determines the jet performance and overall print quality (Tuladhar and Mackley 2008). In biofluids such as saliva and blood, the extensional viscosity is also important. In the case of saliva, the extensional rheology impacts oral health, digestion, and taste perception (Mandel 1993; Schipper et al. 2007), while in blood, the relaxation time can be an indicator of an individual's hematocrit (Sousa et al. 2018) and extensional stresses can cause hemolysis (Down et al. 2011).

A significant advancement in the measurement of the extensional rheology of viscoelastic fluids was the development of a filament-stretching extensional rheometer (FiSER)

✉ Siva A. Vanapalli
siva.vanapalli@ttu.edu

[1] Department of Chemical Engineering, Texas Tech University, Lubbock, TX, USA

[2] Measurement Science, PepsiCo Global Functions Governance and Compliance, Hawthorne, NY, USA

[3] School of Chemical Engineering, The University of Queensland, Brisbane, Queensland 4072, Australia

Published online: 20 May 2019

(McKinley and Sridhar 2002). Its earliest version involved a free-fall extensional viscometer, where a liquid bridge was stretched between two plates at a constant velocity, thus allowing for uniaxial extensional flow (Matta and Tytus 1990). Refinements have been made to this initial approach to induce exponential separation of plates and produce a constant elongational strain rate (Anna et al. 1999; McKinley et al. 2001; Tirtaatmadja and Sridhar 1993). The midplane radius of the filament and the tensile force exerted by the fluid on the plate are measured to determine the extensional viscosity. The FiSER method is well suited for fluids with long relaxation times (e.g., Boger fluids) and not for low-viscosity solutions ($\mu < 1$ Pa/s) with short relaxation times ($< O$ (1 s)) whose liquid bridge would break before a constant strain rate is achieved (Haward 2016; McKinley and Sridhar 2002).

For low-viscosity and weakly elastic polymer solutions, methods based on the thinning of viscoelastic filaments with a free surface have been developed. In the capillary breakup extensional rheometry (CaBER), the elastocapillary thinning dynamics of a free-surface liquid neck are monitored (Bazilevsky et al. 1990; McKinley et al. 2001) and the polymer relaxation time and extensional viscosity are calculated from a model developed by Entov and Hinch (1997). Under its standard operating conditions, the CaBER device can measure the extensional rheology of fluids with relatively low viscosities ($\mu = 2$–10 mPa/s) and relaxation times of several milliseconds (Rodd et al. 2005b). However, with modifications, the limitations imposed by gravitational and inertial effects can be removed and sub-millisecond relaxation times can be measured (Campo-Deano and Clasen 2010).

More recently, the same principles have been used to develop dripping-on-substrate (DOS) rheology (Dinic et al. 2015) where a drop of fluid is slowly dripped from a nozzle onto a substrate and the thinning dynamics are imaged. This configuration simplifies the setup and has been used to quantitate fluid relaxation times as low as milliseconds (Dinic et al. 2017a, b). Another variant of the CaBER method referred to as Rayleigh Ohnesorge jetting extensional rheometry (ROJER) exploits forced-convection capillary-thinning instability to measure elongational properties of low-viscosity and weakly elastic fluids (Ardekani et al. 2010; Keshavarz and McKinley 2016; Keshavarz et al. 2015). Additionally, pulsed surface acoustic waves have been used to create a liquid bridge in low-viscosity fluids, eliminating the need to stretch the bridge between parallel plates (Bhattacharjee et al. 2011).

In contrast with macroscale extensional rheometers, where inertial and gravitational effects can hinder accurate measurements of low-viscosity polymer solutions (Pipe and McKinley 2009), in recent years, there has been significant interest to develop microfluidic extensional rheometers. The interest stems from benefits of microfluidics such as access to high extensional strain rates at low Reynolds numbers due to small length scales, precision control over channel geometry, and ability to visualize kinematics of the imposed flow (Galindo-Rosales et al. 2013; Gupta et al. 2016; Haward 2016).

Current approaches to microfluidic extensional rheometry include cross slot (CS), contraction–expansion (CE), and filament-thinning (FT) devices (Alves 2008). Both the cross slot (Haward et al. 2012) and contraction–expansion (Kim et al. 2018; Ober et al. 2013; Wang and James 2011) devices involve the measurement of the pressure drop versus flow rate relation to quantify extensional viscosity as a function of strain rate. The distinction is that in a CS device, homogeneous strain rate along with large fluid strain can be achieved in the vicinity of the stagnation point, while in the CE device, transient elongational flow is generated and fluid strain is determined by the contraction ratio. In the FT devices, immiscible fluids are used in microfluidic cross- or T-junction devices to create viscoelastic filaments and droplets that self-thin similar to the CABER device (Arratia et al. 2008; Christopher and Anna 2009; Juarez and Arratia 2011; Steinhaus et al. 2007). The FT devices are able to achieve higher strain rates [$\dot{\varepsilon} \sim O$ (100 s^{-1})] than the filament thinning rheometers [$\dot{\varepsilon} \sim O$ (10 s^{-1})], making them suitable for dilute, low-viscosity fluids (Christopher and Anna 2009).

Despite significant advancements being made in developing microfluidic extensional viscometers for weakly elastic fluids in the last decade, there are still some unmet needs. For example, in the CS and CE devices, pressure sensors are used to measure the additional pressure drop due to elastic stresses and these sensing elements are in contact with the flow. Such approaches are not ideal for handling biofluids where use-and-throw capability is desired to avoid laborious washing and sample cross contamination. Likewise, repeated handling of particulate fluids in these devices may become problematic due to adhesion of particles on channel and sensor surfaces, unless rigorous washing protocols are implemented. Also, the sensors are typically mounted on silicon substrates which prevent any flow visualization unless a separate, transparent device is fabricated (Ober et al. 2013). FT devices do not require pressure sensors; however, they use high-speed cameras to visualize the fast elastocapillary thinning process, requiring a sophisticated setup. Therefore, there is a need for a simple and disposable microfluidic extensional viscometer that can facilitate point-of-care rheology.

Previously, we have developed an image-based method to measure shear viscosity (Solomon et al. 2016). This method, which we have coined as the "iCapillary," involves a thin-slit high-resistance linear microchannel connected with a very low-resistance glass capillary. We have shown that this approach provides accurate measurement of shear rheology of polymeric fluids that is in good agreement with macrorheometry. In this study, we apply the iCapillary approach to a microfluidic hyperbolic CE channel design that was optimized previously using computational modeling (Zografos et al. 2016) but was not tested experimentally. We improved our previous approach by replacing the external glass capillary with a molded capillary

channel, thus making the eCapillary a monolithic device. The technical novelty of the eCapillary method compared to existing microfluidic extensional rheometers is in its simplicity; no pressure sensors or other expensive specialty equipment are required, just a commonplace smartphone camera. These features make the eCapillary device disposable and attractive for measuring extensional rheology of biofluids.

The key results of our study are as follows: (i) we identify the operating thresholds for viscoelastic instabilities to occur, thereby defining the regime for extensional viscosity measurements; (ii) using holography-based velocimetry technique, we show that a constant extensional strain rate can be achieved in the CE channel although, in a narrow region of the throat, necessitating a correction for shear contribution to the measured pressure drop; (iii) the onset of extensional thickening was observed to occur at the Deborah number close to unity; and (iv) we compare extensional viscosity data from the eCapillary device with data from other microfluidic studies and show that the data is in good agreement. Such a comparison has not been done previously.

Results

Characterization of shear rheology and relaxation time of polymeric fluids

In this study, we focused on measuring the extensional rheology of polyethylene oxide (PEO) and polyacrylamide (PAM) solutions (see Table 1) which have been previously shown to be low-viscosity and weakly elastic fluids (Dinic et al. 2017b, 2015). We used PEO with a molecular weight (M_W) of 4 MDa, which has an overlap concentration ($c^* \approx 900$ ppm), and varied the concentration ($c = 250$–5000 ppm), to obtain dilute ($c < c^*$) and semi-dilute ($c > c^*$) solutions with water as the solvent. We also prepared PEO solutions of enhanced solvent viscosity by adding 60 wt% glycerol ($\mu = 10$ mPa s). For PAM, we chose 5–6 MDa ($c^* \approx 670$ ppm) and made dilute solutions. Prior to measuring their extensional rheology, we characterized their shear rheology and relaxation times since the properties of these fluids can be sensitive to preparation protocols, shear, and age (Odell et al. 1990). In addition, as discussed further in the section "Determining instability thresholds using streakline imaging," we use the shear viscosity and the relaxation time data to compute the Reynolds number (Re) and Deborah number (De), respectively, to assess the onset of flow instabilities as well as the viscous contribution to the pressure drop (ΔP_V).

Shear viscosity

In Fig. 1, we show the shear rheology data for PEO/water, PEO/glycerol, and PAM/water systems. The data lies above the low torque limit, but below the flow instability threshold of the double gap geometry (Rodd et al. 2005a). We observed an increase in the shear viscosity and the shear thinning behavior as the PEO concentration increased from 250 to 5000 ppm (Fig. 1a). When the solvent was increased to 60 wt% glycerol ($\mu = 10$ mPa s), the shear viscosity was found to increase by nearly 10-fold and behaved like a Boger fluid. Both of the PAM solutions exhibited nearly identical shear thinning behavior, where the shear viscosity was only marginally increased with a concentration increase from 250 to 500 ppm (Fig. 1b). The shear thinning behavior of the PEO and PAM fluids was fitted to a power-law model, and the fit parameters are shown in Table 1. These power-law parameters were used in the computational fluid dynamics (CFD) simulations as discussed in the section "Basic principle and operation of the eCapillary extensional viscometer."

Relaxation time

The extensional relaxation time of the dilute and semi-dilute polymeric fluids was measured using dripping-on-substrate rheology (Dinic et al. 2017a, b, 2015). For this technique, a drop of the elastic fluid was dripped onto a glass substrate where a thin liquid bridge was formed between the dripping nozzle (with radius R_0) and the substrate. The liquid bridge would self-thin and inevitably break, as shown by the image sequence in Fig. 2a. The thinning dynamics of the radius ratio R/R_0 is plotted in Fig. 2b where there is first a power-law decay and then a slower, exponential decay, which corresponds to the inertiocapillary (IC) and elastocapillary (EC) regimes, respectively.

For our study, we focused on the EC regime where the thinning of the liquid bridge is dominated by elastic and capillary stresses. The thinning dynamics of the filament radius ($R(t)$) can be modeled based on a theory for a finite-extensible nonlinear elastic (FENE) fluid (Entov and Hinch 1997)

$$\frac{R(t)}{R_0} \approx \left(\frac{GR_0}{2\sigma}\right)^{\frac{1}{3}} \exp\left[\frac{-t}{3\lambda_E}\right] \tag{1}$$

In Eq. (1), G is the elastic modulus, σ is the surface tension, and λ_E is the relaxation time. Since the radius exponentially decays with time, the relaxation time can simply be calculated from the exponential fit parameters.

The measured relaxation times for each of our polymer concentrations are shown in Fig. 2c. Here, we have three key observations: (i) For PEO, regardless of the polymer concentration or solvent viscosity, we observe an almost linear relationship. We note that for 1 MDa PEO, Dinic et al. (2017a) reported a linear scaling when $c/c^* > 1$ and a power-law scaling of 0.67 when $c/c^* < 1$; however, they did not report a scaling for higher molecular weight PEO and when $c < c^*$. In our study, we used

Table 1 Measured shear and extensional properties of polymer solutions used in the study

Polymer	c (ppm)	c/c^*	λ_E (ms)*	k (Pa/s^n)$^+$	n^+
PEO	250	0.28	10.1 ± 0.4	0.0039 ± 0.0002	0.836 ± 0.011
	500	0.56	19.4 ± 0.5	0.0033 ± 0.0002	0.883 ± 0.012
	750	0.84	26.5 ± 1.8	0.005 ± 0.0004	0.851 ± 0.017
	1000	1.12	33.4 ± 4.2	0.0066 ± 0.0003	0.845 ± 0.012
	2500	2.8	105 ± 9	0.0182 ± 0.0005	0.817 ± 0.011
	5000	5.59	182 ± 18	0.0943 ± 0.0004	0.698 ± 0.011
PEO/Gly	250	0.28	85 ± 17	0.0137 ± 0.001	0.963 ± 0.013
	500	0.56	174 ± 22	0.0157 ± 0.001	0.959 ± 0.017
PAM	250	0.37	3.9 ± 0.5	0.0023 ± 0.0002	0.896 ± 0.020
	500	0.75	5.6 ± 0.3	0.0025 ± 0.0002	0.901 ± 0.012

*Values represent the mean and standard deviation from at least 10 independent measurements

$^+$ Values represent the mean and standard error from the power-law fit of the shear viscosity versus shear rate data

4 MDa PEO, which has been shown to aggregate even in dilute concentrations (Shetty and Solomon 2009); this aggregation could increase the relaxation time of dilute solutions. (ii) When the solvent viscosity for PEO was increased by a factor of 10, the relaxation time for a given concentration increased by nearly a factor of 10 as well. (iii) PAM solutions exhibited a lower relaxation time than PEO, by approximately a factor of 3. This decrease could be caused by the fact that PAM has a nearly three times longer Kuhn segment length, l ($l/l_0 = 2.5$ and 6.5 for PEO and PAM, respectively, where l_0 is the segment length), which causes PAM chains to be stiffer and thus exhibits less elastic behavior (Banerjee and Tyagi 2011).

Basic principle and operation of the eCapillary extensional viscometer

The eCapillary method is based on measuring the relation between the pressure drop (ΔP) and flow rate (Q) of a viscoelastic fluid though a CE microchannel where the flow has both shear and extensional velocity gradients. The pressure drop results from both viscous and elastic stresses, $\Delta P = \Delta P_V + \Delta P_E$, where ΔP_V is the viscous contribution to the pressure drop and ΔP_E is the excess pressure drop due to extensional viscosity. We will verify that there is no other contribution to ΔP (i.e., from viscoelastic instabilities) using flow visualization in the section "Determining instability thresholds using streakline imaging."

It has been previously shown (Ober et al. 2013) that the transient apparent extensional viscosity in elongational flow produced using a CE channel can be defined as

$$\eta^+_{E,app} = \frac{1}{\epsilon_H}\frac{\Delta P_E}{\dot{\varepsilon}_a} \tag{2}$$

where ϵ_H is the Hencky strain and $\dot{\varepsilon}_a$ is the apparent strain rate. Therefore, in order to calculate the extensional viscosity, we

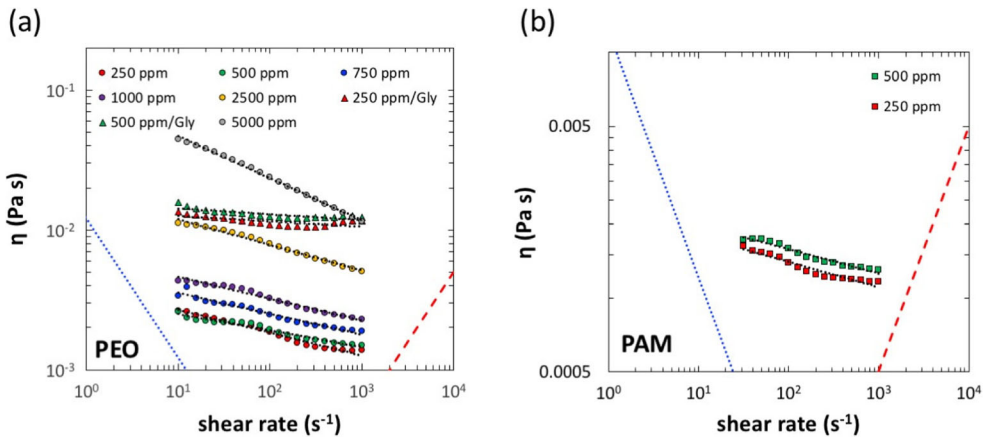

Fig. 1 Shear viscosity of polymeric fluids. The shear viscosity curves as measured using a macrorheometer for **a** PEO (circles) and PEO in 60 wt% glycerol (triangles) and **b** PAM solutions. The power-law fits are shown as dotted lines. The colors red, green, blue, purple, yellow, and gray represent concentrations of 250 ppm, 500 ppm, 750 ppm, 1000 ppm, 2500 ppm, and 5000 ppm, respectively. The blue and red dashed lines represent the low torque and flow instability limits, respectively

first must determine the ΔP_V. There is no exact analytical solution to determine pressure drop in the CE geometry when it is of finite aspect ratio. Hence, three-dimensional CFD simulations were performed to determine the pressure drop caused by a viscous, shear thinning fluid, without accounting for elasticity.

Device geometry

Hyperbolic CE geometries are well suited for studying viscoelastic fluids since they can, in theory, produce a constant nominal strain rate along the centerline of the channel (James et al. 1990). However, several design configurations are possible based on contraction length. Studies have used hyperbolic CE geometries with short-length contraction which do not produce a constant centerline strain rate along the entire contraction length (McKinley et al. 2007; Ober et al. 2013). To alleviate this issue, Zografos et al. (2016) studied computationally several hyperbolic CE designs by varying the channel geometry at the entrance/exit of the CE and identified the hyperbolic CE designs with long-length contractions that would produce a large region of constant centerline strain rate. The optimization strategy involved adding "humps" which resulted in 75% of the contraction length, achieving a constant centerline strain rate (Fig. 3a). However, the suitability of the optimized hyperbolic CE designs for extensional viscosity measurements was not assessed.

In this study, we selected one of Zografos et al.'s 2016 designs which had the best agreement between the encoded and the numerically determined centerline strain rates, as shown in Fig. 3a. The microfluidic CE has a main channel width (w_u) of 800 μm, a contraction width (w_c) of 100 μm, a contraction length (l_c) of 1600 μm, and a height (h) of 110 μm. The capillary sensor channel used to determine Q has a height and width of $h_s = w_s = 3.175$ mm and a length of $l_s = 10$ cm (Fig. 3b). For our CE geometry, the apparent extensional rate along the centerline of the channel is

$$\dot{\varepsilon}_a = \frac{Q}{l_c h}\left(\frac{1}{w_c} - \frac{1}{w_u}\right) \tag{3}$$

The Hencky strain is maximum at the throat of the channel where $\epsilon_H = \ln(w_u/w_c)$.

Operation of the eCapillary extensional viscometer

The basis for the eCapillary extensional viscometer is the quantification of the ΔP–Q relation. The fluid was driven at a constant pressure through the device, and the flow rate was calculated by tracking the interface in the capillary channel, which has a negligible pressure drop (< 0.01%) compared to the microchannel. Figure 3c shows the interface position as a function of time, and the inset shows a time elapse image

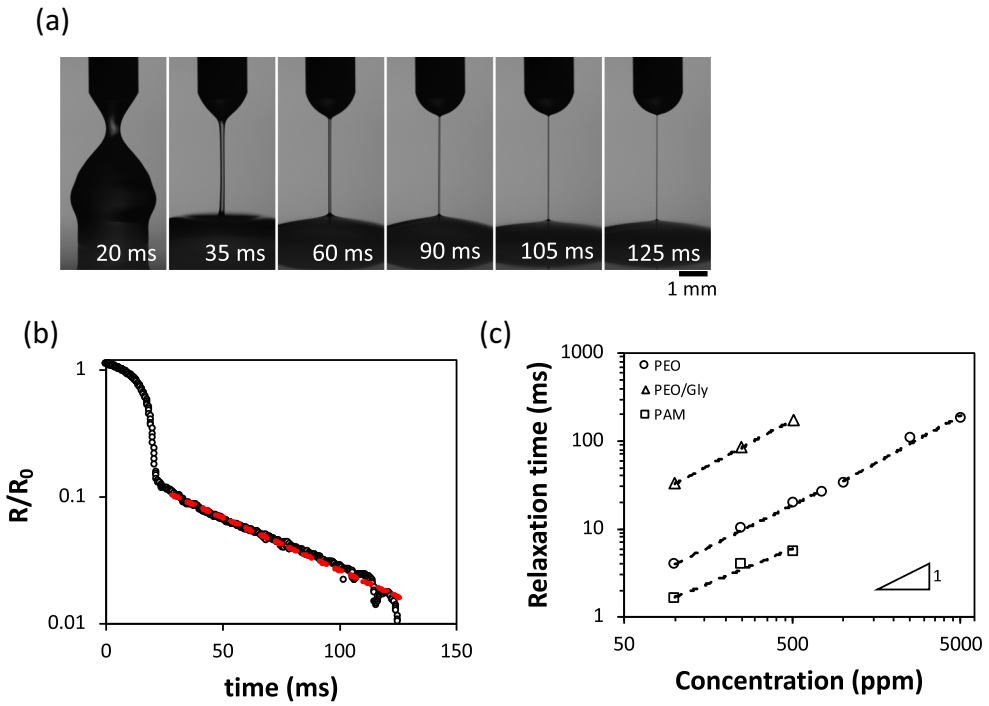

Fig. 2 Relaxation time measurement using the dripping-on-substrate rheology. **a** Time-lapse image sequence and radius thinning of 500 ppm PEO liquid bridge. **b** Radius evolution of thinning filament for the same PEO solution where the elastocapillary regime has been fitted to an exponential decay (Eq. (1)) (red dashed line). **c** Measured relaxation times for PEO (circles), PEO in 60 wt% glycerol (triangles), and PAM (squares). The lines are fit to the data, showing a slope close to unity

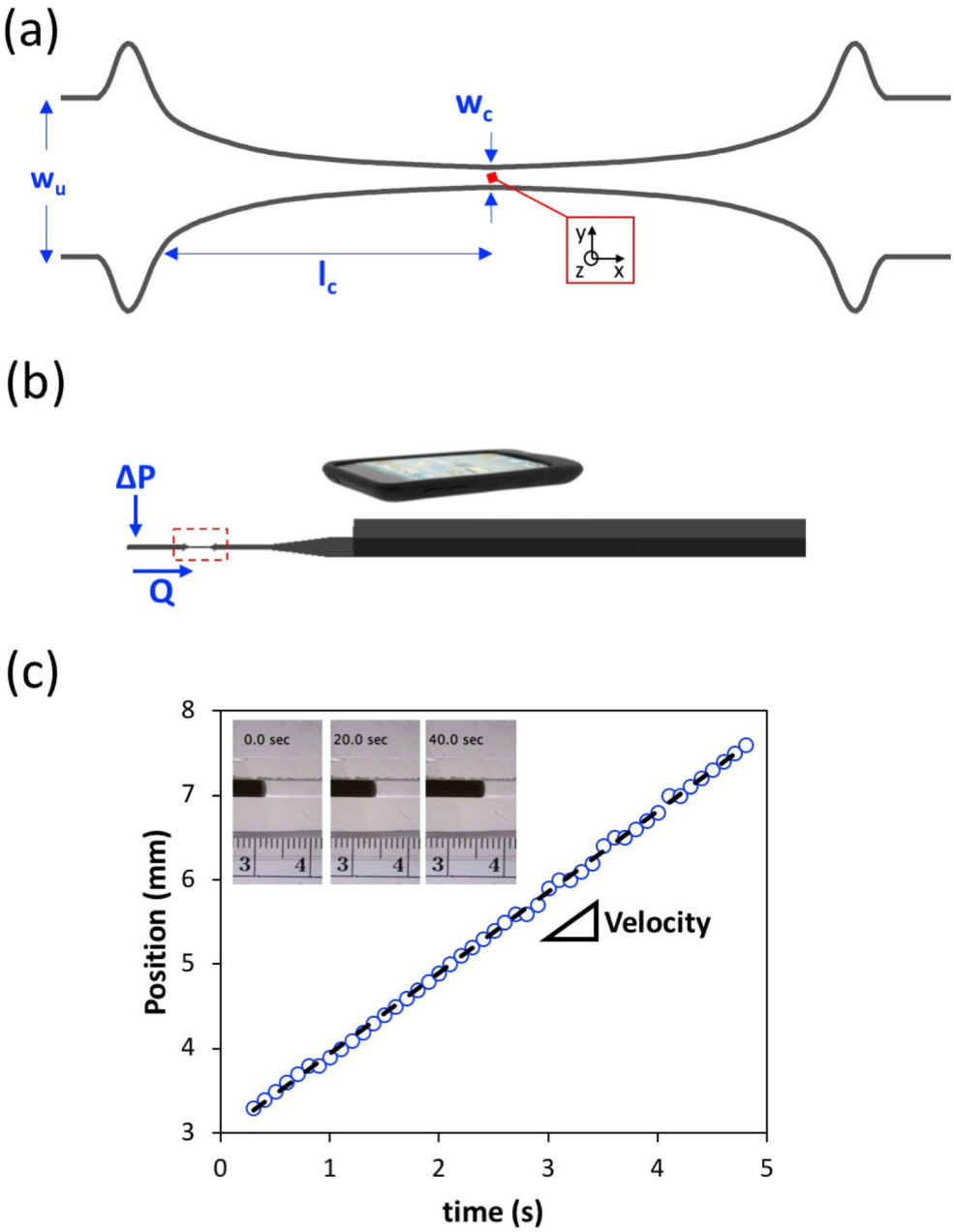

Fig. 3 Basic principle of the eCapillary extensional viscometer. **a** Geometry of the hyperbolic contraction–expansion microchannel. Also shown are the upstream and downstream humps. **b** Measurement setup showing the microfluidic device with a contraction–expansion channel (marked in red) and a capillary sensor channel that is imaged with an iPod camera. **c** Tracking the position of the interface in the capillary channel as a function of time provides the fluid velocity and therefore the flow rate. Inset shows an image sequence for 500 ppm PEO at 10 mbar, imaged at 10 fps

sequence of the fluid movement. We note that dye was added to the polymer solutions to enhance the contrast of the moving interface during image processing.

As previously shown (Keshavarz and McKinley 2016), at high Reynolds number, inertial effects can be present, which would taint extensional viscosity calculations. Therefore, we performed experiments with Newtonian fluids (water–glycerol mixtures) to assess inertial effects in the eCapillary device. Figure 4a shows the normalized pressure drop ($\Delta P/\mu\dot{\varepsilon}_a$) as a function of *Re*; *Re* here is defined as $Re = \rho d_h l_c \dot{\varepsilon}_a/\eta^1$, where ρ is the fluid density, d_h is the hydraulic diameter of the contraction [$d_h = 2hw_c/(h + w_c)$], and η^1 is the viscosity corresponding to a shear rate of 1 s^{-1} for a non-Newtonian fluid and is equal to μ for a Newtonian fluid. The consistency index value (k) shown in Table 1 corresponds to the viscosity of a power-law fluid at a shear rate of 1 s^{-1}. Here, we find a nearly constant normalized pressure drop over the entire range of $Re = 0.2$–100, indicating a negligible contribution of inertial effects to the measured pressure drop in the eCapillary device.

Determination of the viscous pressure drop (ΔP_V)

There is no exact analytical solution available to determine ΔP_V in the CE channel. Previous studies using a microfluidic CE channel for extensional viscosity measurement used a two-dimensional (2D) approximation to determine the viscous

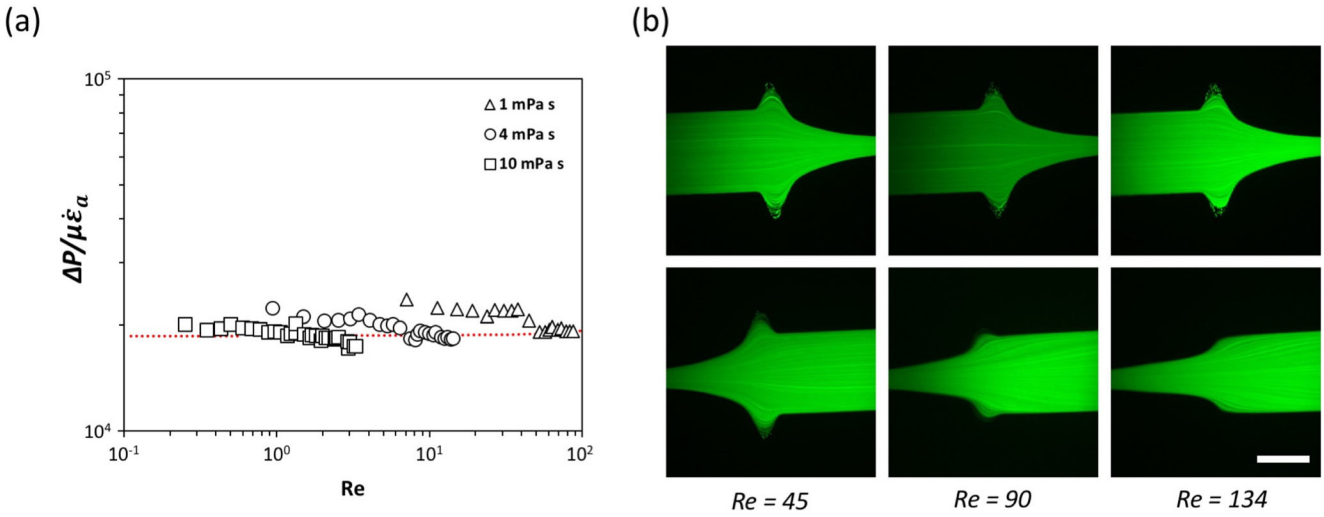

Fig. 4 Characterization of Newtonian flow behavior in the eCapillary device. **a** Normalized ΔP as a function of *Re* for three Newtonian fluids with viscosities of 1 mPa/s (triangles), 4 mPa/s (circles), and 10 mPa/s (squares). The red dotted line represents the normalized ΔP obtained from CFD simulations. **b** Streakline images for water at $Re = 45$ (left), 90 (middle), and 134 (right) at the inlet (top) and outlet (bottom) of the eCapillary microchannel. The scale bar represents 500 μm

contribution (Ober et al. 2013). However, since our channel has an aspect ratio (h/w_c) of ≈ 1, a 2D approximation would underestimate ΔP_V by ≈ 60%. Therefore, we used 3D CFD simulations to compute the viscous contribution to the pressure drop in our CE channel.

We first performed simulations with Newtonian fluids (glycerol mixtures of viscosities 1 mPa/s, 4 mPa/s, and 10 mPa/s) and compared the $\Delta P_V/\mu\dot{\varepsilon}_a$ –*Re* relation with experimental data from the eCapillary (Fig. 4a). We found good agreement (within 3%) between our simulations and experiments, thus validating our simulations. For the polymeric fluids, we implemented the non-Newtonian power-law fluid model using the experimentally obtained power-law indices from the shear rheology data (Table 1). The ΔP_V thus obtained was subtracted from the total pressure drop to determine the excess pressure drop due to extensional viscosity. We note that when $\Delta P_V \approx \Delta P$, the subtraction procedure can result in significant fluctuations. Therefore, in our analysis, we discounted those values where ΔP_E was less than 10% of imposed ΔP.

Determining instability thresholds using streakline imaging

As previously stated, the ΔP in the CE channel is the result of viscous and elastic stresses, and in Fig. 4a, we have shown that there is no appreciable contribution to the ΔP from inertial stresses. However, the ΔP can be contaminated by viscoelastic instabilities which makes the flow kinematics unsuitable for extensional viscosity measurements. Therefore, we used streakline imaging to visualize the flow field and determine at which flow condition, if any, the instabilities occur. The instability onset was characterized in terms of *De* and *Re* where the Deborah number (*De*) is equal to $\lambda_E\dot{\varepsilon}_a$, as shown in Table 2.

We note that the elasticity number ($El = De/Re$) has been used to describe the behavior of viscoelastic fluids (Astarita and Marrucci 1974; Denn and Porteous 1971; McKinley 2005; Ober et al. 2013; Rodd et al. 2007); however, since it is independent of the strain rate, we do not use it to characterize the onset of instability.

First, we confirmed via visualization that there are no appreciable instabilities with a Newtonian fluid in the eCapillary device as anticipated by the pressure drop data in Fig. 4a. At low *Re*, we observed that the streaklines follow the contour of the channel wall and there is no visible crossing of streaks in the direction of flow, from left to right (Fig. 4b). As the *Re* is increased, the flow becomes more focused as it exits the CE, but there is still no observable instability.

For PEO solutions, we imaged the streaklines at the entrance and exit of the CE channel as a function of flow rate, where Fig. 5a shows representative images for 500 ppm from $[De, Re] = [1.3, 3.4]$ to $[De, Re] = [7.7, 20]$. When $De < 3.9$ and $Re < 10$, we observe a stable flow field, similar to the

Table 2 Dimensionless numbers at the onset of instability in the eCapillary device

Polymer	*c* (ppm)	De^*	Re^*
PEO	250	3.6	20.0
	500	3.9	10.1
	750	3.9	5.6
	1000	4.7	3.8
	2500	8.5	1.2
	5000	8.4	0.2
PEO/Gly	250	4.6	1.1
	500	5.4	0.7
PAM	250	1.0	43.6
	500	1.5	35.6

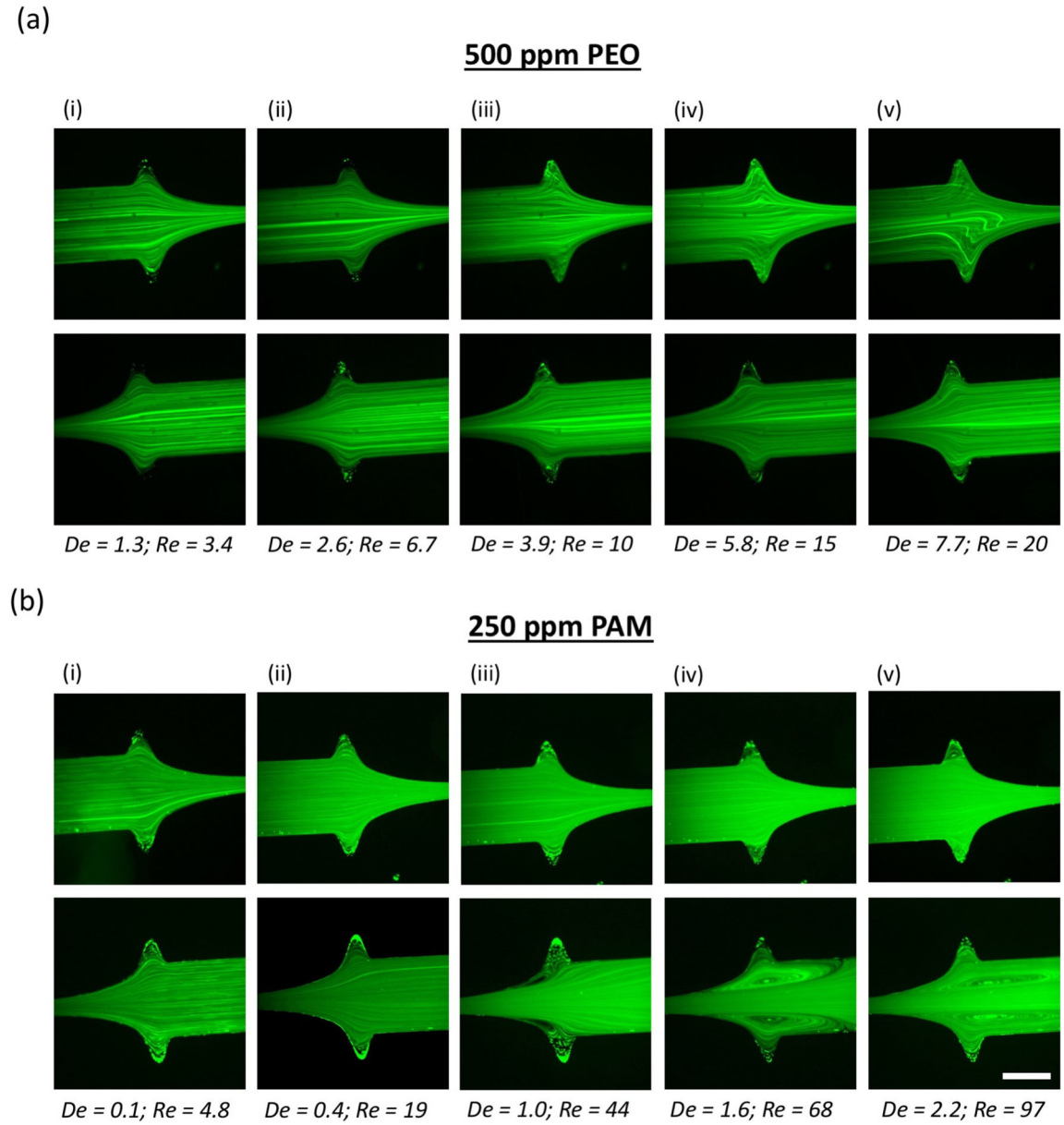

Fig. 5 Flow behavior of polymeric fluids in the eCapillary device. Streakline images for **a** 500 ppm PEO and **b** 250 ppm PAM in the eCapillary microchannel, where the top and bottom rows are the inlet and outlet of CE, respectively, and the fluid was flowing from left to right. The *De* and *Re* are noted below each image pair, and the scale bar represents 500 μm

Newtonian case (Fig. 5a(i and ii)), but the flow becomes unstable beyond these values (Fig. 5a(iii)). The instability becomes even more pronounced as *De* and *Re* are increased (Fig. 5a(iv and v)). Since the instability originates for $De > 1$ and $Re > 1$, it has an inertioelastic character to it, and we observe that it originates in the humps of the CE design, eventually propagating into the contraction channel.

The dimensionless parameters at the onset of instability (Re^* and De^*) for the tested polymeric fluids are summarized in Table 2. Here, we find that as the PEO concentration was increased, the onset of instability occurred at a higher *De* and lower *Re*, making fluids with a higher concentration of PEO more conducive to extensional viscosity measurements. Also, increasing the solvent viscosity by an order of magnitude decreases the Re^* by nearly an order of magnitude, making the PEO/Gly solutions amenable to extensional viscosity measurements. Thus, the data in Table 2 informs on the operating limits for conducting extensional rheometry with PEO solutions. We note that although the eCapillary device is capable of making pressure drop measurements for conditions beyond Re^* and De^*, those data were not included in determination of extensional viscosity of the tested fluids.

For PAM, Fig. 5b shows the streakline images for 250 ppm from [*De*, *Re*] = [0.1, 4.8] to [*De*, *Re*] = [22, 97]. Here, there

are no perceivable instabilities in the inlet of CE channel; rather we observed an inertially dominated instability downstream of the CE channel (Fig. 5b(iii)), which became more pronounced as *Re* was increased (Fig. 5b(v)). For the molecular weights we have chosen, PAM exhibits less elastic behavior than PEO (evident from the relaxation times shown in Table 1), which makes it less susceptible to elastic instabilities. The instability in PAM occurs at $De^* \approx 1$ (Table 2), making this molar mass sample unsuitable for extensional viscosity measurements, since elastic stresses will only dominate when $De > 1$. It is possible to obtain extensional viscosity data of PAM solutions by choosing higher molar mass chains or increasing solvent viscosity.

From our data in Table 2, we have not been able to identify a unique criterion for the onset of instability since we observe the onset to depend on both the Deborah and the Reynolds number. The elasticity number also does not predict well the onset of instability in the hyperbolic contraction–expansion geometry. As a result, the onset of flow instability needs to be determined for every new fluid tested.

Flow field characterization in the eCapillary device

Subsequent to identifying the thresholds for instability, we focused on investigating the kinematics of the flow in the eCapillary device. The hyperbolic CE geometry of the eCapillary device contains both shear and elongational velocity gradients. We therefore mapped the flow kinematics focusing on two objectives: (i) Previously, Zografos et al. 2016 computationally showed that their optimized design which we use can produce a constant centerline strain rate up to $x/l_c = 0.75$, i.e., 75% of the contraction length from the center of the throat. However, this finding has not been verified experimentally. (ii) From an extensional rheometry perspective, given the mixed character of the flow in the CE channel, it is important to determine the region of the throat that is dominated by extensional and shear velocity gradients, justifying the need for correcting shear contribution to the measured pressure drop in the eCapillary device. Here, we address these two objectives using the 250 ppm PEO/water fluid because it is more akin to a Boger fluid and has delayed onset for inertioelastic instabilities compared to other test fluids.

To characterize the velocity field in the hyperbolic CE channel, we used holography-based particle-tracking velocimetry. Digital holography microscopy has the capability to identify tracer particles in 3D image volumes (Salipante et al. 2017; Sheng et al. 2006), thereby enabling determination of 3D flow kinematics. This technique has been used to previously characterize flow fields in microfluidic devices (Choi and Lee 2010; Ooms et al. 2009; Salipante et al. 2017; Satake et al. 2006). Building on these prior works, we used this technique to determine the stream-wise velocity field $u_x(x,y,z)$ with the origin being at the center of the throat (see Fig. 3a). The

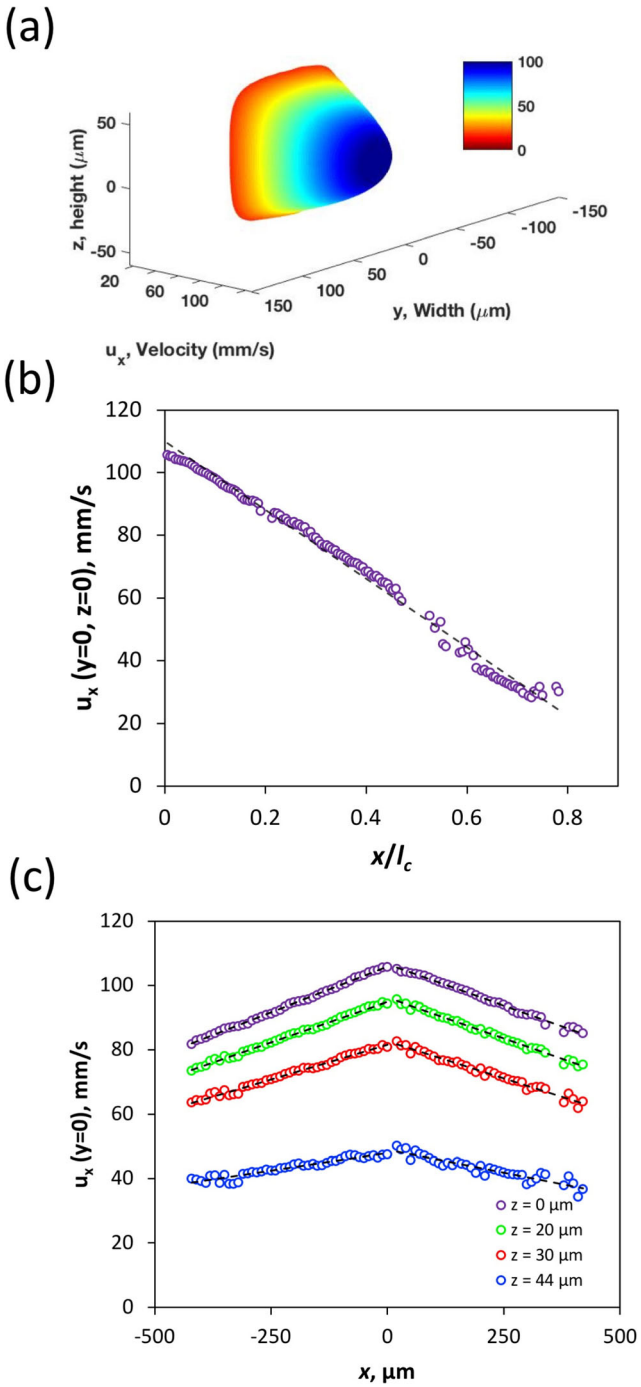

Fig. 6 Flow field characterization in the eCapillary device. **a** Velocity field at the cross section of the CE throat. **b** The centerline axial velocity profile as a function of the normalized downstream distance. **c** The axial velocity at different channel depths (z). The flow rate was 2.42 mL/h

measured velocity field $u_x(x = 0,y,z)$ is shown in Fig. 6a, i.e., at the cross-sectional plane going through origin. As expected, the velocity is maximum at the origin and decays close to the walls. The width-wise and depth-wise velocity profiles are also nearly the same due to the almost square cross section at the throat.

Next, we measured the centerline velocity $u_x(x,y=0,z=0)$ from $x/l_c = 0$ to 0.8. As shown in Fig. 6b, the velocity profile decreases linearly with downstream distance, indicating that the centerline strain rate is constant across the contraction length as predicted by Zografos et al. (2016). We also measured the axial velocity at different depth locations and $y = 0$. As shown in Fig. 6c, the velocity profiles are symmetric and vary linearly with upstream and downstream distance. By performing linear fits to the data, we observe that the strain rate is nearly constant for $z \leq 30$ μm, with only a 10% decrease in the strain rate from the centerline to $z = 30$ μm. At the centerline ($z = 0$), we measured a strain rate of 54 s^{-1}, which was ~ 1.4 times greater than the apparent strain rate, calculated from Eq. (3). Finally, from the velocimetry data, we computed the magnitude of extensional strain rate ($|du_x/dx|$) and shear rate ($|du_x/dy|$) at the throat. We find that about 5% of the region in the throat has extensional strain rates greater than shear rates, indicating that the flow is extension dominated in a very narrow section of the throat. Thus, most of the contraction flow is dominated by shear effects, necessitating the viscous pressure drop correction discussed in the section "Basic principle and operation of the eCapillary extensional viscometer."

We note that the flow rate corresponding to the data in Fig. 6 was 2.72 mL/h corresponding to $De = 0.5$; thus, the results shown are strictly valid for this condition. From the extensional rheometry perspective, it is important to map the kinematics across the explored De range and a wider set of test fluids, warranting additional investigations which will be reported in the future.

Apparent extensional viscosity of PEO solutions

Given that we have identified the onset of instabilities and provided insights into the flow kinematics, we obtained ΔP–Q data for PEO solutions and determined their apparent extensional viscosity. The normalized ΔP as a function of Re for PEO is shown in Fig. 7, where the symbols are the experimentally measured values and the solid lines are from the CFD simulations where only viscous stresses are present. We observe two regimes of behavior. For low pressures, $\Delta P \approx \Delta P_V$, which implies that the viscous stress is dominant. For higher pressures, $\Delta P > \Delta P_V$, and thereby $\Delta P_E > 0$, implying that there are elastic stresses contributing to the pressure drop. Both of these regimes are observed for almost all of the polymer solutions; however, the ΔP at which the transition between the regimes occurs varies based on the concentration and solvent viscosity.

Using Eqs. (2) and (3), we calculated the apparent extensional viscosity as a function of De, since polymer chains are expected to undergo coil–stretch transition when $De > 0.5$ (Larson and Magda 1989), as shown in Fig. 8. We find that for $De < 1$, $\eta^+_{E,app}$ is nearly constant and when $De > 1$, the

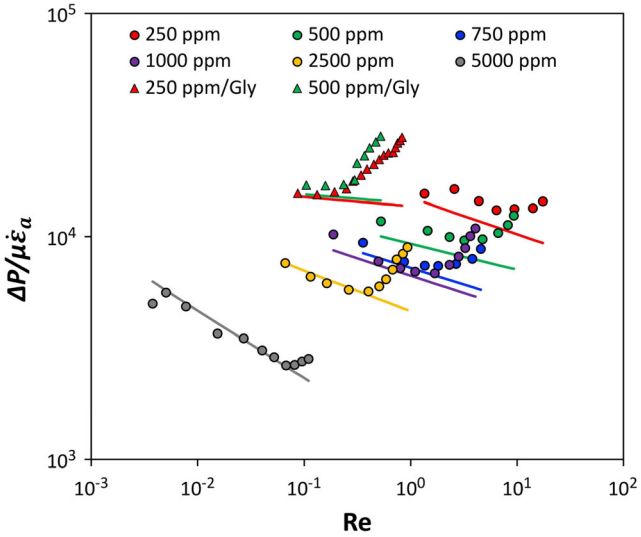

Fig. 7 Normalized pressure drop versus Reynolds number for PEO fluids in the eCapillary extensional viscometer. The experimentally measured ΔP versus Q is shown as points, and the viscous ΔP versus Q calculated from simulations is shown as lines for PEO (circles) and PEO in 60 wt% glycerol (triangles) where the colors red, green, blue, purple, yellow, and gray represent concentrations of 250 ppm, 500 ppm, 750 ppm, 1000 ppm, 2500 ppm, and 5000 ppm, respectively

polymeric fluid undergoes extensional thickening, indicating resistance to elongational stretching of polymer chains. For the higher concentrations (> 1000 ppm), the extensional viscosity decreases with polymer concentration for a given De value. A similar trend is observed when the solvent viscosity is increased where, for a given De, 500 ppm/Gly has a lower $\eta^+_{E,app}$ viscosity than 250 ppm/Gly. Regardless of concentration, the $\eta^+_{E,app}$ is 2–4 orders of magnitude greater than the shear viscosity, exemplifying the importance of measuring this material property.

Comparison with other microfluidic extensional viscometers

As discussed in the "Introduction" section, multiple microfluidic extensional viscometers have been developed; however, to the author's best knowledge, no effort has been made to directly compare the different techniques. In this section, we will compare the results of the eCapillary extensional viscometer to Haward et al.'s (2012) optimized shape cross-slot extensional rheometer (OSCER) and Ober et al.'s (2013) extensional viscometer–rheometer-on-a-chip (EVROC) devices. We will also compare the microfluidic approaches to the DOS rheology reported by Dinic et al. (2017a, b, 2015).

As previously discussed, the extensional viscosity of a viscoelastic fluid depends on fluid composition and kinematic quantities such as strain rate and Hencky strain. In order to compare to Haward et al.'s (2012) and Ober et al.'s (2013)

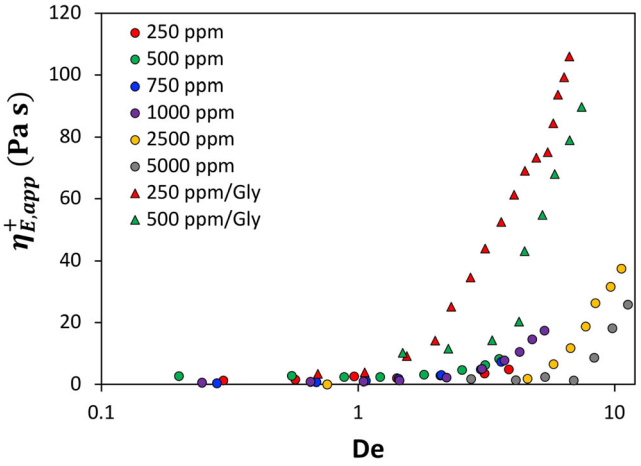

Fig. 8 Apparent extensional viscosity versus Deborah number. The experimentally measured apparent extensional viscosities as a function of the Deborah number are shown for PEO (circles) and PEO in 60 wt% glycerol (triangles) where the colors red, green, blue, purple, yellow, and gray represent concentrations of 250 ppm, 500 ppm, 750 ppm, 1000 ppm, 2500 ppm, and 5000 ppm, respectively

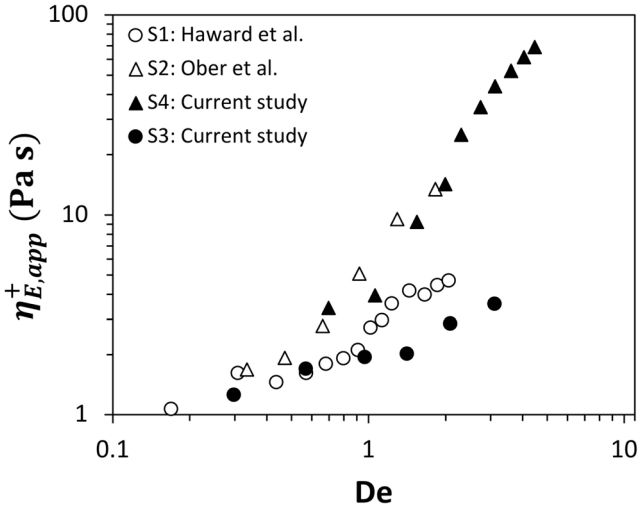

Fig. 9 Comparison of eCapillary measurements with data from the literature. The apparent extensional viscosity as a function of Deborah number is shown for PEO solutions studied by Haward et al. (2012) in the OSCER device (open circles) and by Ober et al. (2013) in the EVROC device (open triangles) along with the 250 ppm (black circles) and 250 ppm/Gly (red triangles) from this study

results, we first note that they tested PEO solutions with different molecular weights, concentrations, and solvent viscosities as shown in Table 3. These variables can be collectively captured in the measured polymer relaxation time. Therefore, we choose to compare the results of our PEO fluids which had comparable relaxation times (see Table 3). In terms of the flow kinematics, the eCapillary and EVROC devices have Hencky strains of ≈ 2 and similar flow fields. However, in the case of the OSCER device, the flow is planar elongational and a unique Hencky strain cannot be determined because it diverges at the stagnation point.

In Fig. 9, we compare the extensional viscosity measurements of Haward et al. (2012) and Ober et al. (2013), whose PEO solutions had relaxation times of 6.5 ms and 76 ms, respectively, with our 250 ppm and 250 ppm/Gly, which had relaxation times of 10.1 ms and 85 ms (Table 3). We find relatively good agreement between our 250 ppm PEO and Haward et al.'s (2012) 500 ppm in glycerol, where the onset of extensional thickening behavior is $De \approx 2$ and ≈ 0.5, respectively. The minor difference in the onset arises due to the different flow kinematics in the two geometries. Interestingly, we observe that our 250 ppm/Gly data nearly overlays with Ober et al.'s (2013) 3000 ppm/Gly measurements, due to the fact that the device geometry and kinematics are similar. For both sets, fluids with a higher relaxation time exhibits more extensional thickening behavior than the lower relaxation time fluids. Overall, we find that the eCapillary device is capable of making the same extensional viscosity measurements but in an easy-to-use, disposable device.

It is interesting to compare existing CE devices and eCapillary for extensional viscosity measurements. Among the CE devices, the extensional viscosity of polymeric fluids has been characterized the most with the EVROC, where the channels are etched in glass and the pressure sensors are mounted on a silicon substrate. Due to the size of the sensors, the contraction channel is larger in dimensions (≈ twice the channel volume) than the eCapillary device. Because of the larger geometry, low-viscosity, dilute polymer solutions are susceptible to inertial instabilities in the EVROC device (Keshavarz and McKinley 2016). In our device, we have shown the ability to measure the extensional viscosity of dilute, low-viscosity ($\mu \sim 2$ mPa s), and weakly elastic ($\lambda_E \sim 4$ ms) fluids.

Table 3 Characteristics of PEO fluids shown in Fig. 8

Sample	M_W (MDa)	C (ppm)	η (mPa s)	λ_E (ms)	ϵ_H	$\dot{\varepsilon}_a$ (s^{-1})	Ref.
S1*	1	500	12.9	6.5	N/A	26–317	Haward et al. (2012)
S2*	2	3000	12.9	76	2	4–24	Ober et al. (2013)
S3+	4	250	1	10.1	2.08	16–570	Current study
S4+	4	250	10	85	2.08	8–78	Current study

*λ_E measured using the CaBER device

+ λ_E measured using the DOS rheology technique, duplicated from Table 1

Additionally, the eCapillary is transparent, enabling easy flow visualization and assessment of the onset of instabilities, which is essential for reliable extensional viscosity measurements. Keshavarz and McKinley (2016), who used the EVROC device in their study, determined the inertia-dominated region using the normalized pressure drop of only Newtonian fluids, which our results show may not be an accurate indicator for inertioelastic instabilities. This study did not report flow visualization results, presumably because of difficulty in imaging flows in a device that is not fully transparent. However, using streakline imaging, we were able to ascertain the presence of inertioelastic instabilities at much lower *Re*.

In this study, in addition to the eCapillary device, we conducted DOS experiments. With the DOS technique, the transient apparent extensional viscosity can be calculated from the thinning dynamics as $\eta^{+}_{\mathrm{E,app}} = \sigma/\dot{\varepsilon}_a R(t)$, where $\dot{\varepsilon}_a = -2d\ln R(t)/dt$. In Fig. 10, we plot the extensional viscosity as a function of Hencky strain, $\epsilon_{\mathrm{H}} = 2\ln[R_0/R(t)]$, where the extensional viscosity for a fluid increases with the Hencky strain and increases with polymer concentration. These trends are similar to those reported by Dinic et al. (2015). Also, we find that when the solvent viscosity is increased by a factor of 10, the extensional viscosity is increased by nearly the same factor. We note that in the EC regime, the liquid bridge thins exponentially, the strain rate is constant for a given fluid, and the Weissenberg number (*Wi*) can be calculated as $\lambda_{\mathrm{E}}\dot{\varepsilon}_a = 2/3$. Therefore, with the DOS technique, extensional viscosity as a function of strain rate cannot be determined. In contrast, in the eCapillary device, as shown in Fig. 8, the extensional viscosity data of polymeric fluids can be obtained as a function of strain rate and at a given Hencky strain.

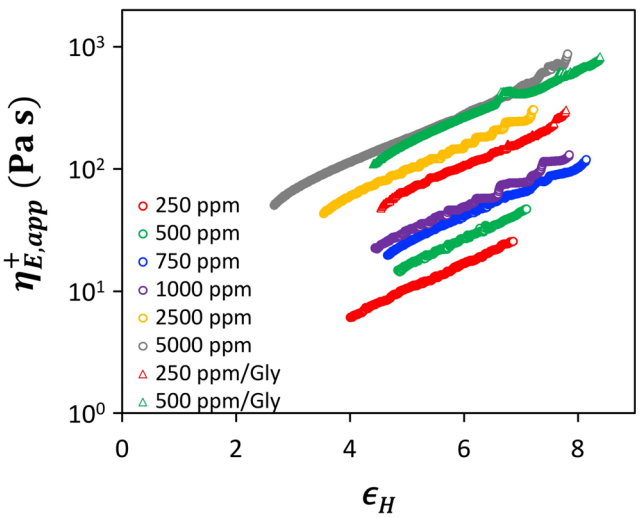

Fig. 10 Apparent extensional viscosity versus Hencky strain. The experimentally measured apparent extensional viscosities as a function of Deborah number are shown for PEO in water (circles) and PEO in 60 wt% glycerol (triangles) where the colors red, green, blue, purple, yellow, and gray represent concentrations of 250 ppm, 500 ppm, 750 ppm, 1000 ppm, 2500 ppm, and 5000 ppm, respectively

Conclusions

In this study, we have developed the eCapillary extensional viscometer which produces elongational flow using a hyperbolic contraction–expansion microchannel. We identified the operating regime based on the onset of viscoelastic instabilities and showed that the device can produce homogeneous extensional strain rate in a narrow section of the throat. We show that ΔP–Q measurements can be made using the low-resistance sensor channel and a smartphone camera. We have shown that this technique is capable of measuring the apparent extensional viscosity of low-viscosity ($\mu = 2$–10 mPa s) and weakly elastic PEO solutions as a function of strain rate. Extensional thickening behavior was observed to initiate at $De \approx 1$ consistent with the coil-to-stretch transition. Our extensional viscosity data agrees with previous microfluidic extensional viscometers.

We have shown that the eCapillary device is an easy-to-use, disposable device that is suitable for extensional rheometry of weakly elastic polymer solutions. We find that an extensional viscosity curve of 10 data points requires 20 min of experimentation time, 20 min for image processing, and 2 mL of sample volume. Such capabilities in a disposable format have not been demonstrated in the literature before. Thus, the eCapillary device has the potential to open new opportunities for studying extensional rheology of biofluids including blood and saliva. Additional improvements to our approach are possible including parallelization since multiple eCapillary channels can be imaged within the field of view of the smartphone camera (Solomon et al. 2016). In addition, the shear rheology can be concomitantly measured by including a linear channel device, next to the CE channel, thereby eliminating the need for macrorheology.

Materials and methods

Device fabrication

A master mold for the eCapillary device was fabricated using standard soft lithography techniques (Xia and Whitesides 1998). First, SU-8 mold of the microchannel ($h = 110$ μm) was made on a 6-in. silicon wafer (University Wafers). Then, an aluminum rod (3.175 mm × 3.175 mm × 100 mm; McMaster Carr) was adhered to the wafer using superglue, where there was a slight overlap (~ 1 mm) with the SU-8 microchannel. Degassed 10:1 monomer:cross-linker polydimethylsiloxane (PDMS) (Sylgard 184, Dow Corning) was poured over the mold and cured at 70 °C for at least 4 h.

Subsequently, the PDMS replicas were cut out from the mold and 1-mm fluidic ports were created (Miltex Biopsy Punches). The replicas were first plasma bonded (Harrick Plasma) to 0.02-in.-thick PDMS sheets (BISCO® HT-6240, Rogers Corporation) and then bonded to two microscope slides (25 mm × 75 mm; Fisher Scientific) for rigidity.

Sample preparation

Stock solutions of 1% PEO ($M_W = 4$ MDa, WSR301, Dow Corning) and 1 wt% PAM ($M_W = 5$–6 MDa, Polyscience) in water were mixed on a benchtop roller (Wheaton), set at 5 rpm, for 4 days until well mixed. Diluted solutions, ranging from 100 to 5000 ppm, with 1% black food dye (McCormick), were prepared fresh each day before experimentation. The PEO/Gly solutions that were made with 60 wt% glycerol (Sigma-Aldrich), 1 wt% black food dye, and the diluted PEO stock solution were mixed on the benchtop roller for at least 2 h until they were well mixed. The same batch was used for the eCapillary, shear rheology, and dripping-on-substrate experiments.

Shear rheology measurements

The shear viscosity versus shear rate measurements were made on an AR 2000 rheometer (TA Instruments). The double-concentric cylinder geometry was used with a gap of 500 μm, and the set temperature was the same as the room temperature where the eCapillary experiments were done, ranging from 20 to 22 °C.

Dripping-on-substrate rheology measurements

The DOS experiments utilized a standard silhouette imaging setup, which consisted of a high-speed camera (Phantom V711) with a macrolens (Nikon Micro-Nikkor 60 mm) and two extension tubes (7 mm and 28 mm), a stainless steel pin as the nozzle (outer diameter, $D = 1.829$ mm, Instech), a syringe pump (PHD 2000, Harvard Apparatus), and a diffused light source. The distance between the glass substrate and nozzle tip (H) was set to be $\sim 3D$. The dripping flow rate was 0.02 mL/min (Dinic et al. 2015), and the drops were recorded at frame rates between 500 and 10,000, depending on their relaxation time.

Dinic et al. (2017a) wrote a MATLAB algorithm that was used to analyze their DOS experiments. We modified the algorithm to include a binary conversion before the liquid bridge radius is measured. Also, we incorporated an exponential curve fitting to the elastocapillary region, which was used to calculate the relaxation time and Hencky strain versus extensional viscosity. The surface tension of each solution was measured using the pendant drop method (Stauffer 1965), and the images were analyzed with a previously written MATLAB algorithm (Bello et al. 2015).

Streakline imaging

For characterizing the onset of instability, we visualized the flow using 0.1 vol% of 1-μm fluorescent microspheres (FluoSpheres™, 2% solids, Thermo Fisher Scientific) added to the diluted solutions. All experiments were done at a constant flow rate using a syringe pump (PHD 2000, Harvard Apparatus). The CE channel was imaged on an inverted microscope (Olympus IX81) equipped with an automated translational stage (Thorlabs) and a CCD camera (Hamamatsu). Images were taken at three locations of the CE channel: its entrance, throat, and exit (Fig. 4) at a × 4 magnification with a frame rate of 10 fps and exposure time of 100 ms.

eCapillary experimental protocol

The experimental setup included a pressure controller (MFCS-Flex, Fluigent, France), the eCapillary device, a light box, an iPod (fifth generation, Apple), and a phone stand. The device was placed on the light box, and the phone stand was placed 9 cm above it. The pressure controller was used to drive the fluid from a sample vial, through a Tygon Microbore tube (0.05 in. and 0.02 in., Cole Parmer) and a 1-mm stainless steel coupler (Instech), to the microfluidic device. The movement of the fluid–air interface was recorded using the FiLMiC Pro app on an iPod. The videos were recorded between 10 and 30 fps, where the interface movement was at least 5 mm and the total length of the video was at least 50 frames.

A custom MATLAB algorithm was written to calculate to the flow rate of the fluid in the capillary channel based on liquid–air interface movement. In the algorithm, each video was converted to binary and the interface position along the centerline of the channel was tracked as a function of time. The position versus time data was fitted to a linear function where the slope was equal to the fluid velocity. This velocity was multiplied by the capillary channel's cross-sectional area to determine the flow rate.

Holography-based particle-tracking velocimetry

To investigate flow kinematics in the hyperbolic CE geometry, we used inline digital holography microscopy (DHM) (Salipante et al. 2017; Satake et al. 2006; Sheng et al. 2006) in conjugation with particle tracking velocimetry (PTV). Our DHM optical setup has been described in detail elsewhere (Singh et al. 2017a, b). The 250 ppm PEO solution was seeded with polystyrene beads (2 μm diameter, Bang Laboratories) and flowed at a rate of 2.42 mL/h. Holograms were recorded

at a distance of 100 μm below the glass bottom of the PDMS microchannel using a high-speed camera (Phantom V711). The frame rate was adjusted so as to allow a maximum displacement of 9–30 μm for the fastest particles, and the imaging was done with a × 20 objective at an effective resolution of 1 pixel/μm over a 512 × 512 field of view. The CE channel was imaged at upstream and downstream locations, and approximately 40,000 holograms were collected per location having ~ 100 particles/hologram.

The holograms were then cleaned using background subtraction and reconstructed using an angular spectrum method (Schnars et al. 2015; Singh et al. 2017b) in a MATLAB environment. The 3D location of the particles' center was determined based on the lateral and transverse intensity profiles (within ± 0.5 μm) from the reconstructed intensity volume. Finally, the velocity gradient tensor (VGT) algorithm (Ishikawa et al. 2000) was applied for particle tracking velocimetry and velocity vectors were calculated in order to get information about the 3D flow kinematics in the entire flow volume. The results of flow kinematic investigation are used for analyzing the strain rates along the streamline in the flow inside the hyperbolic channel. The advantage of DHM is the availability of high-fidelity volumetric information without attenuation of spatiotemporal resolution. As a result, we are able to obtain 3D velocity profiles inside the hyperbolic cross section over large distances.

CFD simulations

ANSYS Fluent (v. 17.1) was used to analytically determine the ΔP–Q relation for our Newtonian and non-Newtonian fluids. We imported our microchannel geometry from AutoCAD (v. 2015, Autodesk), extruded the channel to half the height of our device, and used the bottom surface as a symmetry plane to reduce computational time. For the polymer solutions, we fitted the shear viscosity versus shear rate data to a power-law model and used the flow indices as our parameters in the Non-Newtonian power-law fluid model in Fluent. We ran the simulations at a constant inlet flow rate which were the same flow rates measured from the eCapillary experiments.

Acknowledgements S.K. Baier and R.V Potineni are employed by PepsiCo, Inc. The views expressed in this research article are those of the authors and do not necessarily reflect the position or policy of PepsiCo, Inc.

The authors would like to thank Dr. Jeremy Marston for use of his laboratory equipment for the DOS experiments. We are also appreciative to Prof. Vivek Sharma and Jelena Dinic for providing us with their image processing code for DOS. We would like to acknowledge Ryan Hoang for his assistance with the device fabrication and experimental support. We are also grateful to Prof. Jason Stokes for the useful discussions.

Funding information This project was supported by PepsiCo Inc.

References

Alves M (2008) Design of a Cross-Slot Flow Channel for Extensional Viscosity Measurements. In: AIP Conference Proceedings, vol. 1027, no. 1, pp. 240–242. AIP

Anna SL, McKinley GH (2001) Elasto-capillary thinning and breakup of model elastic liquids. J Rheol 45:115–138

Anna SL, Rogers C, McKinley GH (1999) On controlling the kinematics of a filament stretching rheometer using a real-time active control mechanism. J Non-Newtonian Fluid Mech 87:307–335

Ardekani A, Sharma V, McKinley G (2010) Dynamics of bead formation, filament thinning and breakup in weakly viscoelastic jets. J Fluid Mech 665:46–56

Arratia PE, Gollub JP, Durian DJ (2008) Polymeric filament thinning and breakup in microchannels. Phys Rev E 77:036309

Astarita G, Marrucci G (1974) Principles of non-Newtonian fluid mechanics vol 28. McGraw-Hill, New York

Banerjee S, Tyagi A (2011) Functional materials: preparation, processing and applications. Elsevier, Amsterdam

Bazilevsky A, Entov V, Rozhkov A (1990) Liquid filament microrheometer and some of its applications. In: Third European rheology conference and Golden Jubilee meeting of the British Society of Rheology. Springer, Berlin, pp 41–43

Bello MN, Pantoya ML, Kappagantula K, Wang WS, Vanapalli SA, Irvin DJ, Wood LM (2015) Reaction dynamics of rocket propellant with magnesium oxide nanoparticles. Energy Fuel 29:6111–6117

Bhattacharjee P, McDonnell A, Prabhakar R, Yeo L, Friend J (2011) Extensional flow of low-viscosity fluids in capillary bridges formed by pulsed surface acoustic wave jetting. New J Phys 13:023005

Campo-Deano L, Clasen C (2010) The slow retraction method (SRM) for the determination of ultra-short relaxation times in capillary breakup extensional rheometry experiments. J Non-Newtonian Fluid Mech 165:1688–1699

Choi Y-S, Lee S-J (2010) Holographic analysis of three-dimensional inertial migration of spherical particles in micro-scale pipe flow. Microfluid Nanofluid 9:819–829

Christopher G, Anna S (2009) Passive breakup of viscoelastic droplets and filament self-thinning at a microfluidic T-junction. J Rheol 53: 663–683

Cogswell F (1972) Converging flow of polymer melts in extrusion dies. Polym Eng Sci 12:64–73

Denn M, Porteous K (1971) Elastic effects in flow of viscoelastic liquids. Chem Eng J 2:280–286

Dinic J, Zhang Y, Jimenez LN, Sharma V (2015) Extensional relaxation times of dilute, aqueous polymer solutions. ACS Macro Lett 4:804–808

Dinic J, Biagioli M, Sharma V (2017a) Pinch-off dynamics and extensional relaxation times of intrinsically semi-dilute polymer solutions characterized by dripping-onto-substrate rheometry. J Polym Sci B Polym Phys 55:1692–1704

Dinic J, Jimenez LN, Sharma V (2017b) Pinch-off dynamics and dripping-onto-substrate (DoS) rheometry of complex fluids. Lab Chip 17:460–473

Down LA, Papavassiliou DV, Edgar A (2011) Significance of extensional stresses to red blood cell lysis in a shearing flow. Ann Biomed Eng 39:1632–1642

Entov V, Hinch E (1997) Effect of a spectrum of relaxation times on the capillary thinning of a filament of elastic liquid. J Non-Newtonian Fluid Mech 72:31–53

Galindo-Rosales FJ, Alves M, Oliveira M (2013) Microdevices for extensional rheometry of low viscosity elastic liquids: a review. Microfluid Nanofluid 14:1–19

Gupta R, Sridhar T (1998) Elongational rheometers. In: Rheological measurement. Springer, Berlin, pp 516–549

Gupta S, Wang WS, Vanapalli SA (2016) Microfluidic viscometers for shear rheology of complex fluids and biofluids. Biomicrofluidics 10: 043402

Haward S (2016) Microfluidic extensional rheometry using stagnation point flow. Biomicrofluidics 10:043401

Haward SJ, Oliveira MS, Alves MA, McKinley GH (2012) Optimized cross-slot flow geometry for microfluidic extensional rheometry. Phys Rev Lett 109:128301

Ishikawa M, Murai Y, Wada A, Iguchi M, Okamoto K, Yamamoto F (2000) A novel algorithm for particle tracking velocimetry using the velocity gradient tensor. Exp Fluids 29:519–531

James D, Chandler G, Armour S (1990) A converging channel rheometer for the measurement of extensional viscosity. J Non-Newtonian Fluid Mech 35:421–443

Juarez G, Arratia PE (2011) Extensional rheology of DNA suspensions in microfluidic devices. Soft Matter 7:9444–9452

Keshavarz B, McKinley GH (2016) Micro-scale extensional rheometry using hyperbolic converging/diverging channels and jet breakup. Biomicrofluidics 10:043502

Keshavarz B et al (2015) Studying the effects of elongational properties on atomization of weakly viscoelastic solutions using Rayleigh Ohnesorge jetting extensional rheometry (ROJER). J Non-Newtonian Fluid Mech 222:171–189

Kim SG, Ok CM, Lee HS (2018) Steady-state extensional viscosity of a linear polymer solution using a differential pressure extensional rheometer on a chip. J Rheol 62:1261–1270

Larson R, Magda J (1989) Coil-stretch transitions in mixed shear and extensional flows of dilute polymer solutions. Macromolecules 22: 3004–3010

Mandel ID (1993) A contemporary view of salivary research. Crit Rev Oral Biol Med 4:599–604

Matta J, Tytus R (1990) Liquid stretching using a falling cylinder. J Non-Newtonian Fluid Mech 35:215–229

McKinley GH (2005) Dimensionless groups for understanding free surface flows of complex fluids SOR Rheology Bulletin 74: 6

McKinley GH, Sridhar T (2002) Filament-stretching rheometry of complex fluids. Annu Rev Fluid Mech 34:375–415

McKinley GH, Brauner O, Yao M (2001) Kinematics of filament stretching in dilute and concentrated polymer solutions. Korea-Aust Rheol J 13:29–35

McKinley GH, Rodd LE, Oliverira MS, Cooper-White J (2007) Extensional flows of polymer solutions in microfluidic converging/diverging geometries. J Cent S Univ Technol 14:6–9

Morrison FA (2001) Understanding rheology, topics in chemical engineering. Oxford University Press, New York

Ober TJ, Haward SJ, Pipe CJ, Soulages J, McKinley GH (2013) Microfluidic extensional rheometry using a hyperbolic contraction geometry. Rheol Acta 52:529–546

Odell JA, Muller AJ, Narh KA, Keller A (1990) Degradation of polymer solutions in extensional flows. Macromolecules 23:3092–3103

Ooms T, Lindken R, Westerweel J (2009) Digital holographic microscopy applied to measurement of a flow in a T-shaped micromixer. Exp Fluids 47:941

Pipe CJ, McKinley GH (2009) Microfluidic rheometry. Mech Res Commun 36:110–120

Rodd LE, Scott TP, Boger DV, Cooper-White JJ, GH MK (2005a) The inertio-elastic planar entry flow of low-viscosity elastic fluids in micro-fabricated geometries. J Non-Newtonian Fluid Mech 129:1–22

Rodd LE, Scott TP, Cooper-White JJ, McKinley GH (2005b) Capillary break-up rheometry of low-viscosity elastic fluids. Appl Rheol 15: 12–27

Rodd L, Cooper-White J, Boger D, McKinley G (2007) Role of the elasticity number in the entry flow of dilute polymer solutions in micro-fabricated contraction geometries. J Non-Newtonian Fluid Mech 143:170–191

Salipante P, Hudson SD, Schmidt JW, Wright JD (2017) Microparticle tracking velocimetry as a tool for microfluidic flow measurements. Exp Fluids 58:85

Satake S-I, Kunugi T, Sato K, Ito T, Kanamori H, Taniguchi J (2006) Measurements of 3D flow in a micro-pipe via micro digital holographic particle tracking velocimetry. Meas Sci Technol 17:1647

Schipper RG, Silletti E, Vingerhoeds MH (2007) Saliva as research material: biochemical, physicochemical and practical aspects. Arch Oral Biol 52:1114–1135

Schnars U, Falldorf C, Watson J, Jüptner W (2015) Digital holography. In: Digital holography and wavefront sensing. Springer, Berlin, pp 39–68

Sheng J, Malkiel E, Katz J (2006) Digital holographic microscope for measuring three-dimensional particle distributions and motions. Appl Opt 45:3893–3901

Shetty AM, Solomon MJ (2009) Aggregation in dilute solutions of high molar mass poly (ethylene) oxide and its effect on polymer turbulent drag reduction. Polymer 50:261–270

Singh DK, Ahrens CC, Li W, Vanapalli SA (2017a) Label-free fingerprinting of tumor cells in bulk flow using inline digital holographic microscopy. Biomed Opt Express 8:536–554

Singh DK, Ahrens CC, Li W, Vanapalli SA (2017b) Label-free, high-throughput holographic screening and enumeration of tumor cells in blood. Lab Chip 17:2920–2932

Solomon DE, Abdel-Raziq A, Vanapalli SA (2016) A stress-controlled microfluidic shear viscometer based on smartphone imaging. Rheol Acta 55:727–738

Sousa P, Vaz R, Cerejo A, Oliveira M, Alves M, Pinho F (2018) Rheological behavior of human blood in uniaxial extensional flow. J Rheol 62:447–456

Stauffer CE (1965) The measurement of surface tension by the pendant drop technique. J Phys Chem 69:1933–1938

Steinhaus B, Shen AQ, Sureshkumar R (2007) Dynamics of viscoelastic fluid filaments in microfluidic devices. Phys Fluids 19:073103

Tirtaatmadja V, Sridhar T (1993) A filament stretching device for measurement of extensional viscosity. J Rheol 37:1081–1102

Trouton FT (1906) On the coefficient of viscous traction and its relation to that of viscosity. Proc R Soc London Ser A 77:426–440

Tuladhar T, Mackley M (2008) Filament stretching rheometry and break-up behaviour of low viscosity polymer solutions and inkjet fluids. J Non-Newtonian Fluid Mech 148:97–108

Wang J, James DF (2011) Lubricated extensional flow of viscoelastic fluids in a convergent microchannel. J Rheol 55:1103–1126

Xia Y, Whitesides GM (1998) Soft lithography. Annu Rev Mater Sci 28: 153–184

Zografos K, Pimenta F, Alves M, Oliveira M (2016) Microfluidic converging/diverging channels optimised for homogeneous extensional deformation. Biomicrofluidics 10:043508